Electronic Supplementary Material (ESI) for RSC Advances


# Supporting information

## Near-infrared luminescent hybrid materials-PMMA doped with neodymium complex: synthesis, structure and photophysical properties

Weizuo Li, Pengfei Yan,* Guangfeng Hou, Hongfeng Li and Guangming Li*

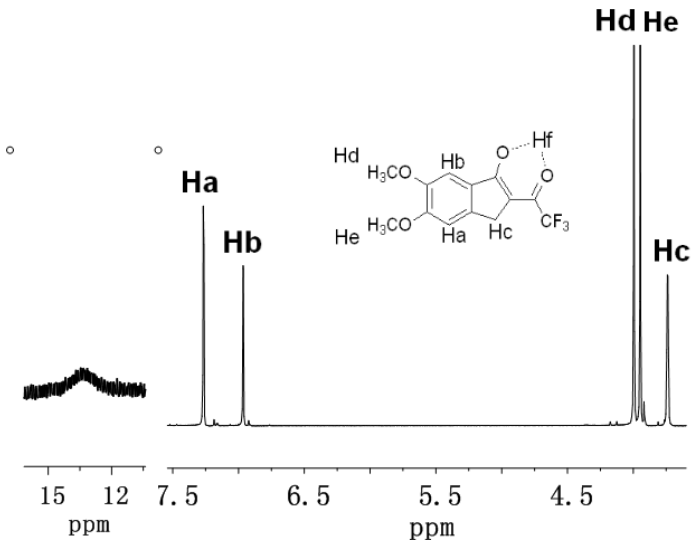


**Fig. S1** 400 MHz $^1$H NMR spectrum of 5,6-DTFI in $CDCl_3$.

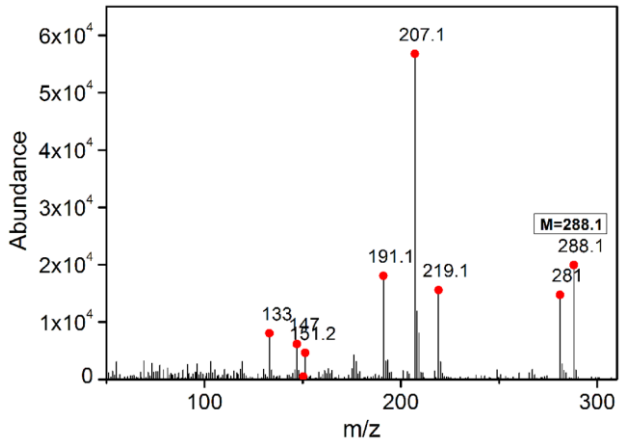


**Fig. S2** Expanded regions of the EI-MS of 5,6-DTFI in acetone.

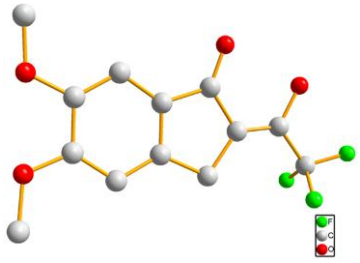

**Fig. S3** Molecular structure of 5,6-DTFI. (All hydrogen atoms have been omitted for clarity)

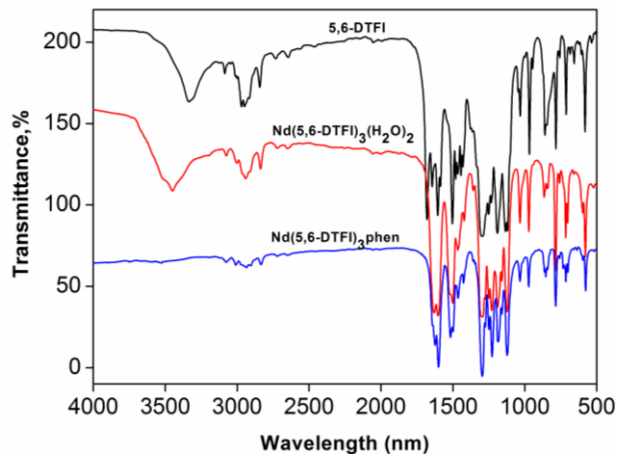


**Fig. S4** IR spectra of ligand, complexes Nd(5,6-DTFI)$_3$($H_2O$)($CH_3OH$) (**1**) and Nd(5,6-DTFI)$_3$(Phen) (**2**).

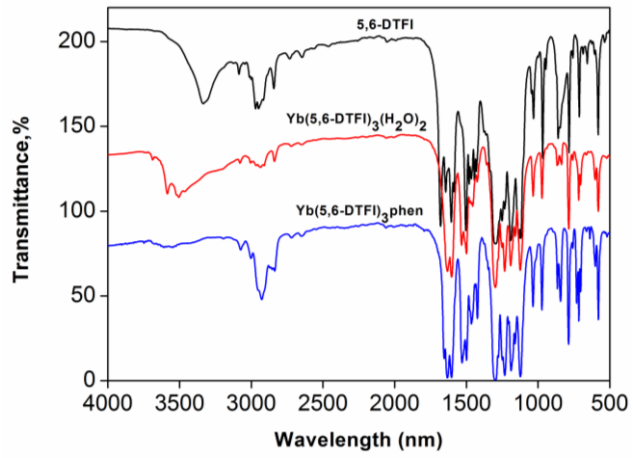


**Fig. S5** FT-IR spectra of ligand, complexes Yb(5,6-DTFI)$_3$($H_2O$)$_2$ (**3**) and Yb(5,6-DTFI)$_3$(Phen) (**4**).

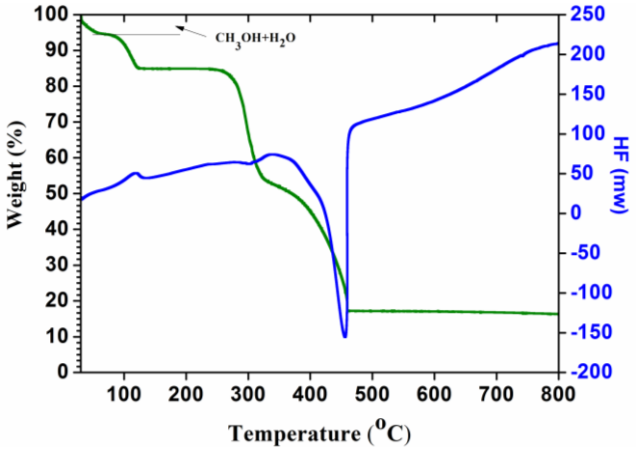


**Fig. S6** TG-DSC curve for the complex **1**.

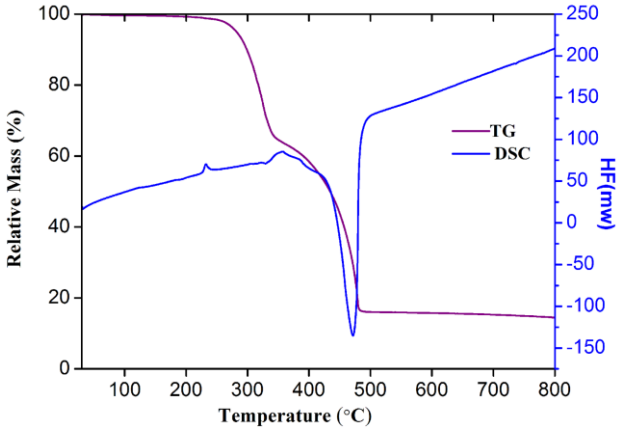


**Fig. S7** TG-DSC curve for the complex **2**.

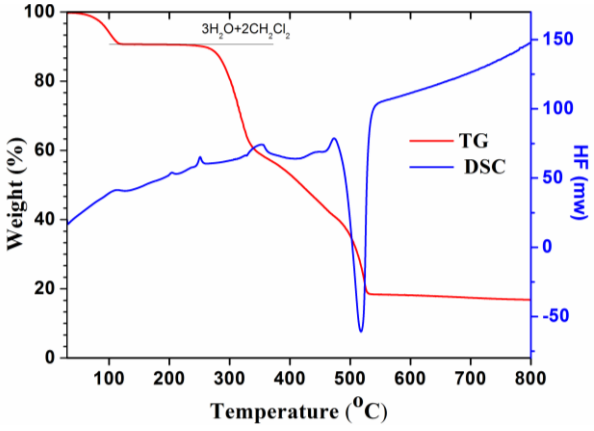


**Fig. S8** TG-DSC curve for the complex **3**.

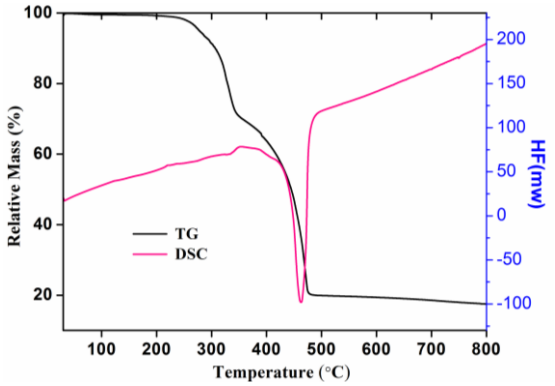


**Fig. S9** TG-DSC curve for the complex **4**.

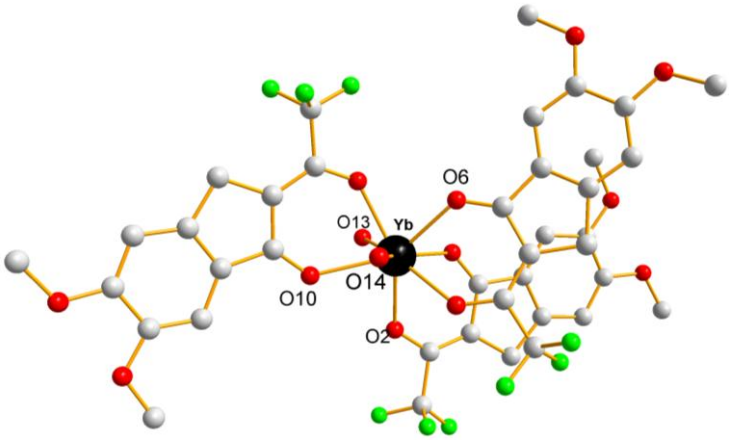


**Fig. S10** Molecular structure of complex **3** (All hydrogen atoms have been omitted for clarity).

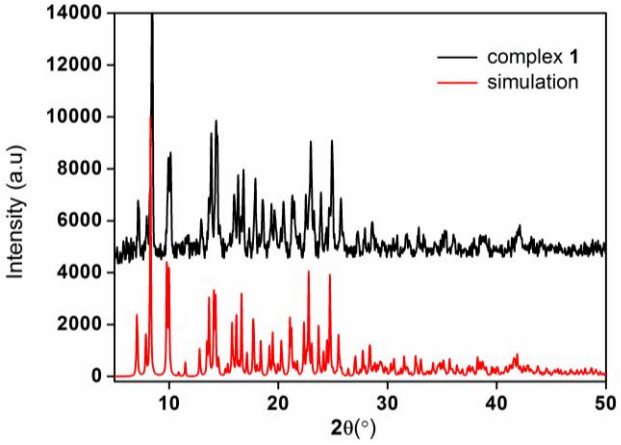


**Fig. S11** Experimental X-ray powder pattern of microcrystalline sample and simulated pattern of **1**.

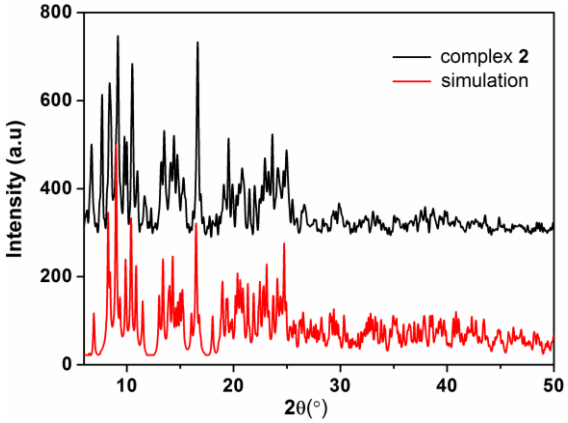


**Fig. S12** Experimental X-ray powder pattern of microcrystalline sample and simulated pattern of **2**.

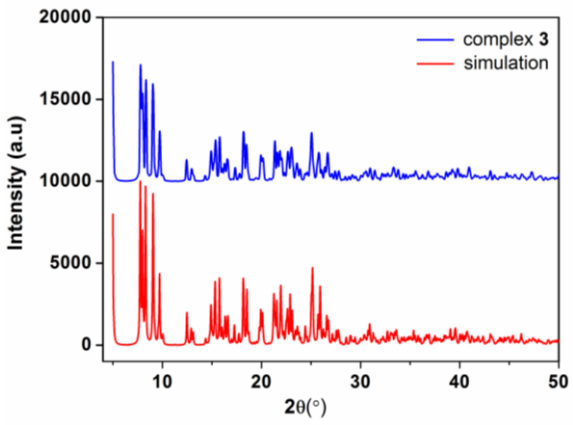


**Fig. S13** Experimental X-ray powder pattern of microcrystalline sample and simulated pattern of **3**.

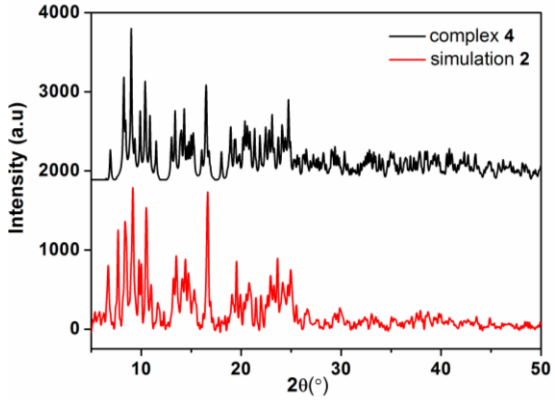


**Fig. S14** Experimental X-ray powder pattern of microcrystalline sample **4** and simulated pattern of **2**.

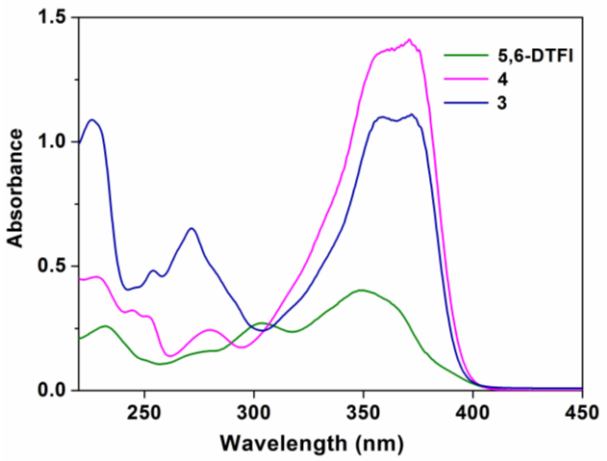


**Fig. S15** UV–vis absorption spectra of 5,6-DTFI, complexes **3** and **4** in $CH_3CN$ solution (c = $1 \times 10^{-5}$ M).

**Table S1** Selected bond length (Å) and angles (º) for complexes **1**–**3**

| **1** | | **2** | | **3** | |
|---|---|---|---|---|---|
| Nd(1)–O(1) | 2.405(3) | Nd(1)–O(1) | 2.390(4) | Yb(1)–O(1) | 2.309(5) |
| Nd(1)–O(2) | 2.416(4) | Nd(1)–O(2) | 2.424(3) | Yb(1)–O(2) | 2.337(4) |
| Nd(1)–O(5) | 2.383(4) | Nd(1)–O(5) | 2.412(4) | Yb(1)–O(5) | 2.305(5) |
| Nd(1)–O(6) | 2.425(3) | Nd(1)–O(6) | 2.447(4) | Yb(1)–O(6) | 2.313(4) |
| Nd(1)–O(9) | 2.488(3) | Nd(1)–O(9) | 2.428(4) | Yb(1)–O(9) | 2.285(5) |
| Nd(1)–O(10) | 2.419(3) | Nd(1)–O(10) | 2.407(3) | Yb(1)–O(10) | 2.378(4) |
| Nd(1)–O(13) | 2.537(4) | Nd(1)–N(4) | 2.645(5) | Yb(1)–O(13) | 2.602(6) |
| Nd(1)–O(14) | 2.535(3) | Nd(1)–N(5) | 2.658(4) | Yb(1)–O(14) | 2.586(6) |
| O(1)–Nd(1)–O(2) | 71.34(11) | O(1)–Nd(1)–O(2) | 71.23(12) | O(1)–Yb(1)–O(2) | 74.01(16) |
| O(5)–Nd(1)–O(6) | 72.51(13) | O(5)–Nd(1)–O(6) | 70.86(12) | O(5)–Yb(1)–O(6) | 75.40(16) |
| O(9)–Nd(1)–O(10) | 70.69(11) | O(9)–Nd(1)–O(10) | 71.47(12) | O(9)–Yb(1)–O(10) | 75.63(15) |
| | | N(4)–Nd(1)–N(5) | 61.68(14) | | |

**Solution-state luminescent properties of complexes 1–4**

The NIR luminescence of the complexes **1**–**4** have been investigated in acetonitrile. For complexes **1** and **2**, the emission spectra (Fig. S16 left) consists of three bands at 894, 1060, and 1328 nm, which are attributed to the f–f transitions $^4F_{3/2} \rightarrow {}^4I_{9/2}$, $^4F_{3/2} \rightarrow {}^4I_{11/2}$ and $^4F_{3/2} \rightarrow {}^4I_{13/2}$, respectively. Among them, the band at 1060 nm is

dominant. For complex **3** and **4**, the emission spectra contains one band corresponding to the $^2F_{5/2}\rightarrow{}^2F_{7/2}$ transition (Fig S16 right). This band is split into three components where the strongest is centered at 975 nm and the weaker two at 1009 nm and 1030 nm, which are attributed to the f–f transitions $^4F_{5/2}\rightarrow{}^4I_{7/2}$.

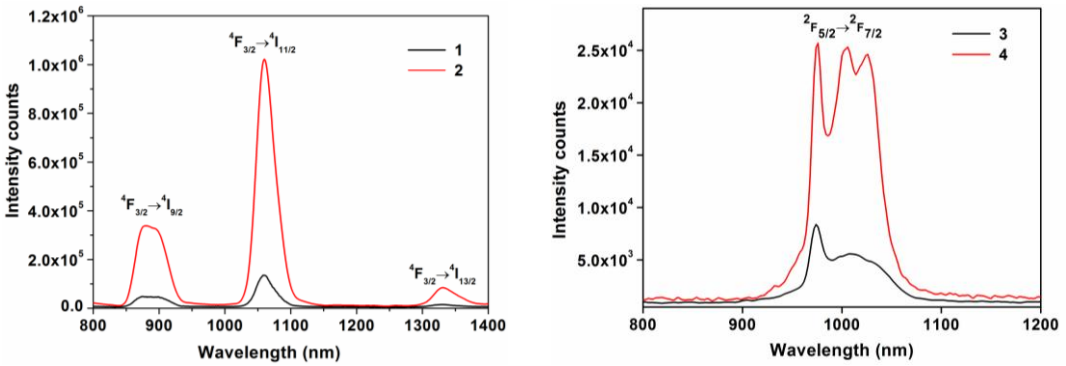


**Fig. S16** Room temperature emission spectra of complexes **1**, **2** (left) and complexes **3**, **4** (right) excited at 410 nm.

The absorption spectra of complexes **3** and **4** (Fig. S17) show that the excited state $^2F_{5/2}$ of $Yb^{3+}$ is likely to split into three levels in samples. The integrated absorption cross section, the spontaneous emission probability and the stimulated emission cross section for $Yb^{3+}$ were calculated using the method adopted by Weber *et al.*[1] the $^2F_{5/2}\rightarrow{}^2F_{7/2}$ transition of $Yb^{3+}$ includes not only the electric dipole transition but also the magnetic dipole transition. The absorption cross section $\sigma_{abs}$ is given by

$$\sigma_{abs} = \frac{2.303\log(I_0 / I)}{Nl} \quad (1)$$

Where log ($I_0/I$) is absorbance, $l$ is the sample thickness and $N$ is the concentration of $Yb^{3+}$ ions. The concentrations of $Yb^{3+}$ ions were calculated from the densities and the batch composition of samples. The absorption cross section was integrated for the absorbed band range of the $^2F_{5/2}\rightarrow{}^2F_{7/2}$ transition

$$\sum_{abs} = \int \sigma_{abs}(\lambda)d\lambda \quad (2)$$

Where $\sum abs$ is the integrated absorption cross section, Spontaneous emission probability (A) is determined by

$$A = \frac{32}{3}\frac{\pi c}{\lambda^{-4}} n^2 \sum_{abs} \quad (3)$$

Where $\bar{\lambda}$ is the mean wavelength of the absorption band and *n* is the refractive index at the mean wavelength. Therefore, the radiative lifetime (τ) is determined by

$$\tau = 1/A \qquad (4)$$

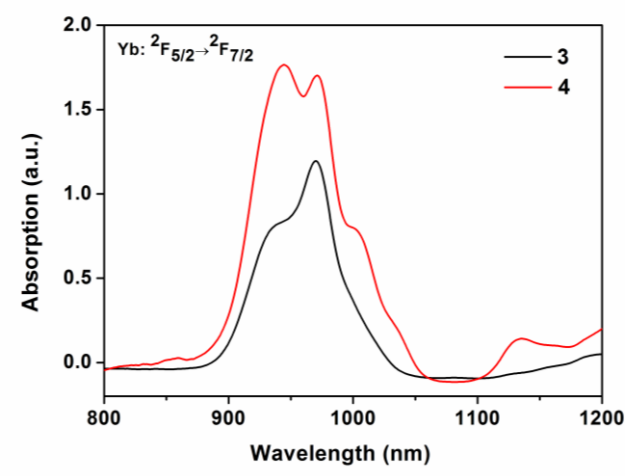


Fig. S17 Absorption spectra of the $^2F_{5/2} \rightarrow {}^2F_{7/2}$ transition of $Yb^{3+}$ in complexes **3** and **4** in solid-state at 298K.

(1) M. J. Weber, J. E. Lynch, D. H. Blackburn and D. J. Cronin, *J. Quantum Elect.*, **19**, 1602.